Electrical Power and Energy Systems 122 (2020) 106173

Contents lists available at ScienceDirect

Electrical Power and Energy Systems

journal homepage: www.elsevier.com/locate/ijepes

Novel modulated equivalent model of point-to-point LCC-based high voltage AC/DC/AC system for geomagnetic storm-induced unbalanced harmonic studies

Tohid Shahsavarian[a,b], Yang Cao[a,b], Emmanouil Anagnostou[c,d], Roderick Kalbfleisch[e]

[a] Electrical Insulation Research Center, Institute of Materials Science, University of Connecticut, Storrs, CT 06269, United States
[b] Department of Electrical & Computer Engineering, University of Connecticut, Storrs, CT 06269, United States
[c] Eversource Energy Center, Innovation Partnership Building, 159 Discovery Drive, Storrs, CT 06269, United States
[d] Department of Civil and Environmental Engineering, University of Connecticut, Storrs, CT 06269, United States
[e] Substation Technical Engineering, Eversource Energy, 107 Selden Street, Berlin, CT 06037, United States

ARTICLE INFO

Keywords:
Geomagnetic disturbance
HVDC grids
Harmonic disturbances
Transformer half-cycle saturation
Line-commutated converters

ABSTRACT

Geomagnetically induced currents have been recognized as significant factors in causing power transformer saturation and damage to other key components of the power system via the injection of a wide range of harmonics to the system. Non-characteristic harmonics owing to transformer saturation during geomagnetic storms generates a wide range of reflected harmonics in HVDC/HVAC grids which cannot be filtered using conventional passive filters. These harmonics depending characteristic impedance of adjacent grid can be damped or amplified. Due to the nonlinear nature of converters, assessing the impact of each injected harmonics on the generation of different frequency components requires complete circuit analysis on both AC and DC sides, the complexity of which often necessitates mitigation solutions beyond a simple converter filter design. This work aims to introduce a novel numerical model to represent the HVDC system's reaction for all harmonic components from disturbances. Also, accurate calculations have been provided to obtain time-variant transferred impedance by the modulation process of 12-pulse bridge converters behind the converter transformer. With proper parametrization of the converter and grid, this model enables the analysis of the whole system without requiring further calculations on the HVDC side. The impact of the commutation overlap angle has been studied thoroughly in this work. The accuracy of proposed model was verified by comparing the results obtained from a direct impedance method and fully-controlled LCC model in Electromagnetic Transient Program (EMTP) for both single and multiple injected harmonic scenarios. Grid voltage and current values at different frequencies for similar harmonic injection scenarios using the proposed reflected equivalent circuit and EMTP model were obtained and compared.

1. Introduction

Half-cycle saturation of power transformers due to flowing of quasi-dc geomagnetically-induced currents (GICs) through their neutral and ground connections has been recognized as the main cause of harmonic generation in power grid [1]. In addition, a significant increase of asymmetric magnetization current as a result of these induced currents increases demanded reactive power by transformers, which in turn causes voltage instability throughout the system [2]. Large non-sinusoidal excitation current of transformers leads to odd and even harmonic generation. Given that these induced currents can affect the grid in large-scale, the researchers have attempted to introduce AC system models to investigate impact of induced current on power grid operation. In [3], GIC models for two EPRI 20-bus and UIUC 150-bus cases were implemented in MATGMD and grid parameters were formulated for a uniformly applied electric field; additionally, DC analysis results were verified using PowerWorld simulator. In [4], performance and accuracy of different methods for geoelectric field calculation were studied by comparing calculated GIC values with observations from a geomagnetic storm that occurred in September 2017. Boteler et al. have proposed a benchmark test case by combining formulas for the synthetic geomagnetic field variation and the earth transfer function for both the uniform and layered models [5]. It provides exact analytic expressions for the geoelectric fields required as an input for grid analysis. Additionally, the effect of the 3-D earth conductivity model compared to the 1-D model was assessed. The coast effect has been

E-mail address: yang.cao@uconn.edu (Y. Cao).

https://doi.org/10.1016/j.ijepes.2020.106173
Received 13 December 2019; Received in revised form 12 April 2020; Accepted 6 May 2020

focused on in some research works and has shown significant impact on earth conductivity model. For instance, the quantitative influence of the coast effect in the 3-D earth conductivity model on predicted GIC was studied in [6] and shows a 23% error between recorded GIC data in Ling'ao nuclear power plant and the model without considering the coast effect. This error drops to 2.9% for the proposed model with the coast effect.

Since saturation of transformers is a commonly reported incident during geomagnetic storm of differing intensity, harmonic analysis has to be provided by power system models introduced for geomagnetic disturbance (GMD) studies. The modified version of the IEEE 118-bus benchmark for time-domain simulation of GMD within an electromagnetic transient program has been adopted in [7,8]. This model enables harmonic analysis as well as AC power system's dynamic response to a GMD. However, the impact of transformer and generator heating has not been taken into account. The power system equipment thermal limits were assessed in [9], and a comprehensive approach was presented to incorporate these limits in the short term and in the long term. It also emphasized high risk of failure of generators due to the effective negative current sequence during a GMD.

In [10], the impact of superimposed DC current excitation in a 550 MVA autotransformer prone to GIC was evaluated for on-load and no-load conditions and demonstrated using different numerical models. This study also shows the spectrum of harmonic contents for different assigned DC injection currents. EPRI has been conducting research in evaluating the impact of harmonics on critical power components and assessing the vulnerabilities of specific equipment against GICs in the power system [11]. Main impacts of this phenomenon include the malfunction of traditional relays such as electromechanical and solid-state relays which are undesirably sensitive to harmonics, failure of capacitor banks without harmonic overload protection, rotor heating and mechanical vibration of turbine-generators for undesirable frequencies and negative sequence harmonic components, and tripping of AC filters in the HVDC/AC grid [12]. Overload protection of equipment has to be carefully evaluated and designed at the grid system level as strengthening individual equipment could worsen performance of other components in the system and hence the entire grid. For example, tripping off capacitor banks or filters equipped with overload protection could result in a significant decrease in reactive power desperately needed by converters during the overload. Therefore, practical and effective harmonic analysis for the HVDC grid and particularly the AC-connected DC grid is critically needed for GICs protection.

Line-Commutated Converter (LCC) based point-to-point HVDC links have been used widely for bulk power transmission throughout the world. The pros and cons of this technology are mainly related to the thyristors used in this topology. LCCs are capable of transmitting bulk power (GW) at high voltage levels (>500 kV); on the other hand, they are sensitive to grid voltage instability and require strong AC systems with a high short circuit ratio. Thyristor-based LCC technology has been used in the majority of HVDC projects around the world [13]. That being the case, failure of these links during a geomagnetic storm would bring forth substantial voltage instability problems, as in the case of the geomagnetic storm reported on March 13, 1989 [14]. Capacitor banks and AC/DC filters employed in HVDC systems are not immune from the wide spectrum of harmonics generated during GIC. Some low-order odd and even harmonics stimulated by GIC-saturated transformers could cause impedance resonances that lead to amplification of harmonic voltages at converter stations. Inverters at the ending terminal are vulnerable to harmonics especially in LCC topology because commutation margin and extinction angle are controlled strictly at the converter station. Voltage distortion can reduce these margins and cause unsuccessful commutation of thyristors, known as *commutation failure*. Moreover, voltage distortion and phase imbalance due to injected harmonics disturb the equidistant firing of switches. The firing control module of the inverter monitors the commutation margin by measuring the extinction angle, maintaining it in a predefined margin by reducing the firing angle of its switches. This causes the reduction of DC-link voltage. Suffice it to say, analysis of harmonic interaction and their impact on the whole AC and DC system is the most critical issue in the hardening of the HVDC grid against GMD.

The time-variant and nonlinear nature of the HVDC converter requires complex analysis to comprehend the interaction of voltage and current signals at its primary and secondary sides, considering all frequency components in the voltage and current signals. The converter transfer function has been presented in many studies to clarify the influence of switching and AC/DC grid parameters on the reflection of harmonic components in the normal operation or in the presence of disturbances in the power system. Extensive analysis of converter behavior has been presented in [15] by numerical methods including the effects of steady and variable commutation periods. Analytical models for 6 and 12 pulse converters have been developed based on modulation theory to show transferred harmonics between AC and DC sides of converters. In [16], analysis results were compared with simulation results for different scenarios. In [17], three-phase dynamic phasor models of HVDC systems for symmetrical and unsymmetrical faults were developed based on modulation theory and corresponding converter switching functions. The study examines the presence of specific harmonics over DC link voltage and AC grid currents.

The mitigation of GICs using different types of blocking devices has already been investigated by EPRI and reported in [18]. In [19], a transformerless power electronic-based compensator connected to the neutral point of a single-phase distribution transformer was proposed as an alternative to a traditional neutral capacitive blocking device to suppress the DC current and regulate the load voltage. However, utilizing blocking devices has not generally been accepted for protecting large-scale grid.

Due to the wide spectrum of harmonic orders generated by saturated transformers during a geomagnetic storm, AC and DC-side harmonic filters are not always sufficient to mitigate all the harmonics generated in the system. The majority of these filters are designed to cancel out characteristic harmonics generated by converters switching under normal operation of the HVDC system; however, another set of harmonic filters are needed to mitigate non-characteristic harmonics generated due to the non-ideal nature of the disturbances. For instance, broadband-type filters were used at the Radisson substation in Quebec for damping specific harmonics during geomagnetic storms [14]. It is worth noting that the magnitude of harmonic components is significantly affected by network impedance characteristics including harmonic filters and transmission lines. Therefore, it is highly probable that some unfiltered harmonics arising from transformer saturation are amplified to cause significant damages in converters and the tripping of the protection equipment in the HVDC link. Even though studies have been done to illustrate the interaction of AC and DC systems, and voltage and current harmonics, the majority of the introduced algorithms are based on a two-sided AC/DC system's current and voltage equations to show the interaction of AC and DC systems and the impact of switching patterns on observed harmonic spectrum in single converter systems, especially voltage source converters (VSCs). In some studies, the converter impedance model for an AC/DC grid was proposed. However, an impedance-modulation analysis for AC/DC/AC systems including sending and receiving converter stations has not yet been studied.

In contrast to previous works, the aim of this paper is to provide a direct calculation of the impedance modulated by both converters, rectifier, and inverter in a HVDC system by considering a complete model of the 12-pulse converter and the three-winding converter transformer used in this configuration. The proposed modulated model of point-to-point LCC-based high voltage AC/DC/AC system provides a toolbox for analysis of instability arising from injected harmonics of saturated transformers during geomagnetic storms. The proposed modulated model also addresses the impact of reflected harmonics from the DC side in our dynamic model, which should be considered in

targeted filter designs to improve performance for all existing harmonics.

The contents of the paper are organized as follows: first, the concept of self-modulation and cross-modulation in the context of high voltage AC/DC/AC system is explained with analytical expressions in Section 2. In Section 3, the frequency and time-dependent equivalent modulated-impedance model of the system has been deduced by analyzing switching modes of a 12-pulse converter – with and without considering the commutation overlap between switches. Section 4 provides more detailed study results based on the simulated model in EMTP and a proposed numerical equivalent model in MATLAB. Obtained results are discussed later in Section 4. The developed analytical method is used to extract the equivalent modulated circuit seen from the AC network including modulation process of rectifier and inverter to highlight its tool strength for GMD instability analysis and AC filter design.

2. Harmonic modulation through 12-pulse converters

In 12-pulse bridge converter topology, two six-pulse bridges are connected in series through a three-phase (or three single-phase) three-winding star/star/delta configuration which provides less harmonics by applying 30° phase shift between the secondary star and tertiary delta three-phase voltages. These voltages can be modulated based on modulation theory and previously defined switching functions (given in Eqs. (1)–(3)) to present continuous switching patterns in each six-pulse bridge. Switching functions are defined to represent reflected phase voltage across each pair of switches contributed in output DC voltage. Fig. 1 depicts how the product of two signals (switching functions and three-phase voltages) generates the output voltage in each six-pulse bridge converter, where by disregarding commutation overlap angle, constant firing angle for switches has been considered. To implement bipolar configuration, two independent sets of same configuration are connected in series on the DC side and in parallel on the AC side, each with its own control module. This configuration can transmit twice the amount of power in comparison to the monopolar configuration for a given rated DC voltage and current.

DC voltage through the modulation of two sets of three-phase AC voltages can be deduced from the following equation:

$$u_{dc} = [u_{3\varphi_{star}}]\cdot[S_{u_s}]^T + [u_{3\varphi_{delta}}]\cdot[S_{u_d}]^T \tag{1}$$

AC voltages ($u_{3\varphi_{star}}$ and $u_{3\varphi_{delta}}$ as three-phase voltages at secondary and tertiary windings of converter transformer) and switching functions (S_{u_s} for secondary star winding side and S_{u_d} for tertiary delta winding side) are used in this equation are as follows:

$$[u_{3\varphi_{star}}] = \left[U_m\sin(\omega t)\;\; U_m\sin(\omega t - \tfrac{2\pi}{3})\;\; U_m\sin(\omega t + \tfrac{2\pi}{3})\right]$$

$$[u_{3\varphi_{delta}}] = \left[U_m\sin(\omega t \pm \tfrac{\pi}{6})\;\; U_m\sin(\omega t - \tfrac{2\pi}{3} \pm \tfrac{\pi}{6})\;\; U_m\sin(\omega t + \tfrac{2\pi}{3} \pm \tfrac{\pi}{6})\right] \tag{2}$$

$$[S_{u_s}]^T = \begin{bmatrix} \sum_{n=1}^{\infty} A_n cosn(\omega t - \alpha - \varphi_c) \\ \sum_{n=1}^{\infty} A_n cosn(\omega t - \alpha - \varphi_c - \frac{2\pi}{3}) \\ \sum_{n=1}^{\infty} A_n cosn(\omega t - \alpha - \varphi_c + \frac{2\pi}{3}) \end{bmatrix}$$

$$[S_{u_d}]^T = \begin{bmatrix} \sum_{n=1}^{\infty} A_n cosn(\omega t - \alpha - \varphi_c \pm \frac{\pi}{6}) \\ \sum_{n=1}^{\infty} A_n cosn(\omega t - \alpha - \varphi_c - \frac{2\pi}{3} \pm \frac{\pi}{6}) \\ \sum_{n=1}^{\infty} A_n cosn(\omega t - \alpha - \varphi_c + \frac{2\pi}{3} \pm \frac{\pi}{6}) \end{bmatrix} \tag{3}$$

where $A_n = (\frac{4}{n\pi})\sin(\frac{n\pi}{2})\cos(\frac{n\pi}{6})(\frac{1}{2} + \frac{1}{\sqrt{3}}\cos(\frac{n\pi}{6}))\cos(\frac{n\mu}{2})$, U_m is voltage peak value, and α, φ_c and μ are the firing angle, voltage intersection angle, and commutation overlap angle introduced in [15], respectively.

For an unbalanced system, three-phase voltages can be decomposed into positive, negative and zero sequences (as explained in [23]), and used in Eq. (1). The same method can be used for both independent rectifiers and inverters to find voltages on their DC side. Theoretically, given DC voltages and DC link impedance, DC current can be calculated. Similar modulation functions can be used to convert not only AC voltages to DC voltage but also DC current to AC currents as follows:

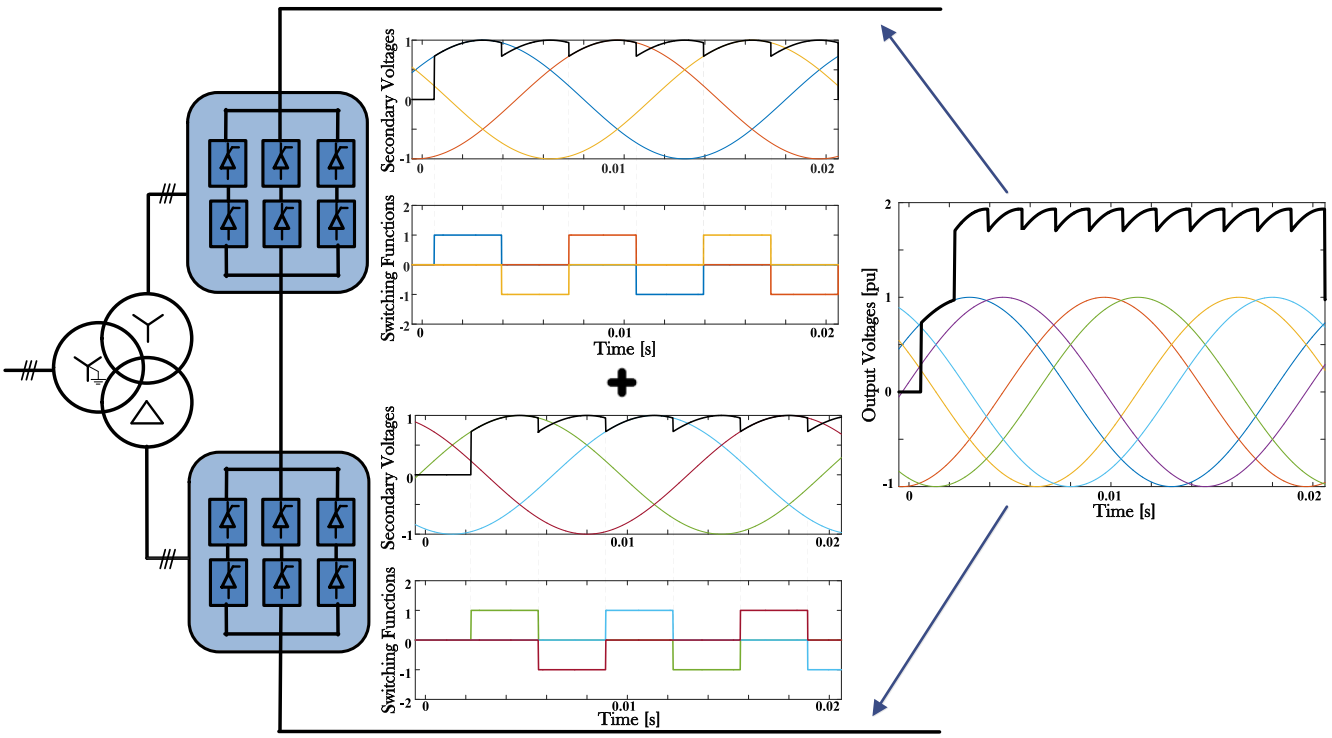

Fig. 1. Modulation of typical 12-pulse monopolar converter for one cycle.

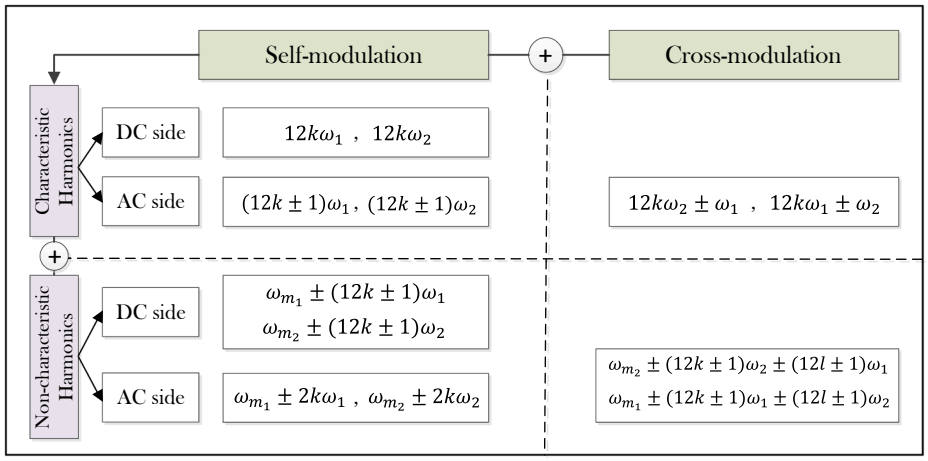

Fig. 2. Categorized generated harmonics on both AC and DC grid.

$$\begin{bmatrix} i_a \\ i_b \\ i_c \end{bmatrix} = \begin{bmatrix} S_{is_a} + S_{id_a} \\ S_{is_b} + S_{id_a} \\ S_{is_c} + S_{id_a} \end{bmatrix} \cdot i_{dc} \tag{4}$$

…where $S_{is}$and $S_{id}$are current switching functions defined for three phases and were already achieved by defining the linear rising function during commutation [14]. As a result, coefficients of Fourier series for current switching functions are defined as follows:

$$A_n = \left(\frac{4}{n\pi}\right)\cdot\sin\left(\frac{n\pi}{2}\right)\cdot\cos\left(\frac{n\pi}{6}\right)\left(\frac{1}{2} + \frac{1}{\sqrt{3}}\cos\left(\frac{n\pi}{6}\right)\right)\cdot\sin\left(\frac{n\mu}{2}\right)/\frac{n\mu}{2} \tag{5}$$

where μ is the same commutation overlap angle defined previously. Also, there is $\pm\frac{\pi}{6}$ radian phase shift between current switching functions because of the secondary and tertiary winding configuration used in the abovementioned voltage switching functions.

Two main groups of harmonics can be generated in normal switching modulation of converters: characteristic harmonics and non-characteristic harmonics, which are found on the AC and DC sides in the presence of disturbances such as unbalanced phase voltages and grid harmonics. These harmonic groups have been categorized in Fig. 2. Self-modulated harmonics are those generated by each converter due to harmonics on their AC or DC side; cross-modulated harmonics are modulated harmonics on the AC side of the converter due to harmonics generated in remote end converter when the frequency of AC grids connected through the DC link is different (ω_1, ω_2). It should be noted that based on the three port network model proposed by Larson [17], depending on the harmonic sequence of ω_m, either harmonic components $\omega_m + (12k \pm 1)\omega$ or $\omega_m - (12k \pm 1)\omega$ will be modulated on the DC side as a harmonic one order higher than the negative sequence harmonic on the AC side and one order lower than the positive sequence harmonic on AC side. Also, cross-modulation of harmonics can produce inter-harmonics in AC grid. These cross-modulated harmonics are more noticeable when DC network impedance is low, especially in a back-to-back converter configuration.

3. Equivalent AC side commutated time-dependent HVDC grid model

In general, studies done in HVDC grid harmonic analysis can be divided into two groups. A first group of authors have provided mathematical modeling for converter modulation to evaluate generated harmonics on both sides of the converter and assess the interaction of the AC/DC system [16,20,21]. Another group of authors have focused on equivalent harmonic impedance obtained by modulation theory to analyze harmonic instability and filter design in the HVDC grid [22–24]. Generation of harmonic voltages and currents caused by half-cycle saturation of power transformers introduces a variety of frequency components that might disturb normal operation of the controller system of converters, along with other components due to the switching modulation process. Vulnerability of the AC system during GMD to these harmonics depends on the behavior of network characteristic impedances which should be considered prior to filter design to avoid unexpected tripping of power system components due to series and parallel resonance. Accordingly, an analytical equivalent modulated impedance model is developed in this section. Impedance modulation has been carried out in two steps explained separately in the following subsections. First, the remote end AC grid is transferred to the DC side. Then, the reflection of the total DC grid is obtained on the primary AC side, by considering complete switching modes in the presence of converter transformer, and the equivalent circuit has been obtained based on the proposed method.

3.1. Commutated impedance through inverter switching seen on DC side

Two switching states can be defined in this conversion process for a 12-pulse converter:

- Two valves are conducting in each 6-pulse converter bridge. By assuming equal AC impedances for three phases, $4Z_{ac}$ will be seen on the DC side.
- During commutation overlap between switching states, parallel-connected impedances of two phases and impedance of the other phase will be seen on the DC side, which is $1.5Z_{ac}$. In each switching step, commutation overlap happens only in one of the upper and lower bridges so the total impedance seen by the DC side will be $3.5Z_{ac}$ (see Fig. 3).

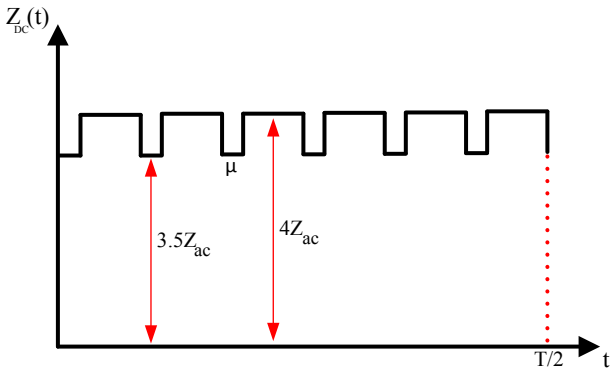

Fig. 3. -Transferred AC impedance to DC side in 12-pulse converter.

Fourier series of this time-varying impedance function can be obtained to represent its frequency components on DC side as follows:

$$Z_{DC}(t) = Z_{ac}\left[\left(4 - \frac{3\mu}{\pi}\right) - \sum_{n=1}^{\infty}(1/n\pi)\sin(6n\mu)\cos(12n\omega t)\right] \quad (6)$$

where Z_{ac} is the equivalent phase impedance of each bridge in the 12-pulse converter as expressed in [22]. In [22], modulated impedance has been presented for the unsymmetrical AC side impedance and is used to obtain the DC network current. It has been shown that unbalanced commutation impedance and overlap angle generate even harmonic components. Accurate calculation of DC current based on time-varying modulated impedance is essential for low DC link impedance in back-to-back configuration to present proper harmonics and inter-harmonics in system. The impact of considering commutation overlap with respect to full transferred time-variant impedance representation seen on DC side of the converter has been compared in [22]. Since the overlap commutation angle is much lower than conduction periods, time-dependent components of order $12n$ in this equation are negligible with respect to the constant term. Based on the presented results, the error of ignoring commutation overlap on the impedance seen on DC side in a remote converter for a AC/DC/AC configuration is considered trivial and can acceptably be neglected for the purposes of this study.

3.2. Commutated impedance through local converter switching seen on the primary side of a three-windings converter transformer

By having an equivalent-impedance of the modulated impedance of a remote end converter and DC link impedance, the modulation process in a local converter is examined in this section to obtain the total impedance seen at the point of common coupling (PCC) on the primary side of converter transformer where AC filters are deployed. Representation of sequence networks for this circuit is difficult due to different connection modes of two sets of three-phase windings on the converter side during switching process. Different switching conduction states have been analyzed with and without considering commutation overlap in two separate sections below. Phasor analysis has been carried out in all calculations.

3.2.1. Modulated impedance calculation on AC side disregarding commutation overlap

The configuration depicted in Fig. 4 has been considered to obtain transferred impedance on the primary side of transformer. Twelve connection modes occur during switching process in each cycle. Although induced currents through the primary windings are not the same in each time interval, a similar induction pattern will be seen for each winding in each period. Table 1 shows different connection modes among valves of upper and lower bridges. In this table $V\angle\theta$ and a represent phase "a" voltage across primary winding and turn ratio of transformer, respectively.

Because of the unbalanced connection of DC impedance across converter side windings, the following general relation between windings is used to calculate induced primary three-phase currents.

$$E_p I_p = E_s I_s + E_T I_T \quad (7)$$

where E_p, E_s, and E_T are the induced voltages across windings which will be the same for all connection modes. I_s and I_T are obtained for each mode using Kirchhoff's circuit laws. I_p is easily obtained through Eq. (7). Generally, three states can be identified from all switching modes which will induce different magnitude of currents for each phase. For phase a, these three states are 1,2,7,8 (state 1); 3,6,9,12 (state 2); and 4,5,10,11 (state 3) within which modes 1,3,4 have been shown in Fig. 5.

The difference between first and second states in induced primary current in phase "a" is the current through phase "a" in the tertiary winding. Induced primary current in phase "a" at the third state is only from current flowed through the phase "a" winding in the tertiary connection.

As can be seen from Table1, the summations of voltages across upper and lower bridges in each mode have the same magnitude in each $\frac{\pi}{6}$ radian conduction period for each pair of switches which are rotating counterclockwise. Therefore, the magnitude of current flowing into the DC grid will be the same and the induced currents for each group of states on the primary side (I_m) can be obtained as follows:

$$I_m^{s1} = \frac{(2\sqrt{3}+4)\cos\left(\frac{\pi}{12}\right).\, a^2 V}{|Z_{DC}|}\angle\left(\theta - \frac{(2m-3)\pi}{12} + \gamma_z\right) \quad (\mathrm{m} = 1, 2, 7, 8) \quad (8)$$

$$I_m^{s2} = \frac{(2\sqrt{3}+2)\cos\left(\frac{\pi}{12}\right).\, a^2 V}{|Z_{DC}|}\angle\left(\theta - \frac{(2m-3)\pi}{12} + \gamma_z\right) \quad (\mathrm{m} = 3, 6, 9, 12) \quad (9)$$

$$I_m^{s3} = \frac{2\cos\left(\frac{\pi}{12}\right).\, a^2 V}{|Z_{DC}|}\angle\left(\theta - \frac{(2m-3)\pi}{12} + \gamma_z\right) \quad (\mathrm{m} = 4, 5, 10, 11) \quad (10)$$

where m and γ_z are the mode number given in the first column of Table 1 and the phase angle of DC impedance, respectively. The

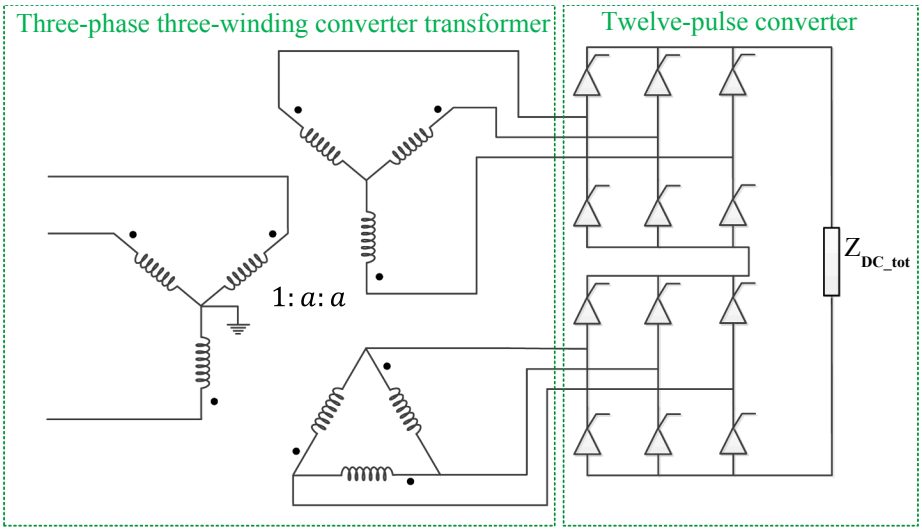

Fig. 4. Converter model connected to converter transformer.

Table 1
Switching modes in each period without commutation overlap.

Connection modes	Secondary winding's phases			Tertiary winding's phases			Voltage across upper bridge	Voltage across lower bridge
	a	b	c	a	b	c		
1	1	−1		1	−1		$\sqrt{3}aV\angle\theta - \pi/6$	$\sqrt{3}aV\angle\theta - \pi/6$
2	1		−1	1	−1		$\sqrt{3}aV\angle\theta + \pi/6$	$\sqrt{3}aV\angle\theta - \pi/6$
3	1		−1	1		−1	$\sqrt{3}aV\angle\theta + \pi/6$	$\sqrt{3}aV\angle\theta + \pi/6$
4		1	−1	1		−1	$\sqrt{3}aV\angle\theta + \pi/2$	$\sqrt{3}aV\angle\theta + \pi/6$
5		1	−1		1	−1	$\sqrt{3}aV\angle\theta + \pi/2$	$\sqrt{3}aV\angle\theta + \pi/2$
6	−1	1			1	−1	$\sqrt{3}aV\angle\theta + 5\pi/6$	$\sqrt{3}aV\angle\theta + \pi/2$
7	−1	1		−1	1		$\sqrt{3}aV\angle\theta + 5\pi/6$	$\sqrt{3}aV\angle\theta + 5\pi/6$
8	−1		1	−1	1		$\sqrt{3}aV\angle\theta + 7\pi/6$	$\sqrt{3}aV\angle\theta + 5\pi/6$
9	−1		1	−1		1	$\sqrt{3}aV\angle\theta + 7\pi/6$	$\sqrt{3}aV\angle\theta + 7\pi/6$
10		−1	1	−1		1	$\sqrt{3}aV\angle\theta + 3\pi/2$	$\sqrt{3}aV\angle\theta + 7\pi/6$
11		−1	1		−1	1	$\sqrt{3}aV\angle\theta + 3\pi/2$	$\sqrt{3}aV\angle\theta + 3\pi/2$
12	1	−1			−1	1	$\sqrt{3}aV\angle\theta - \pi/6$	$\sqrt{3}aV\angle\theta + 3\pi/2$

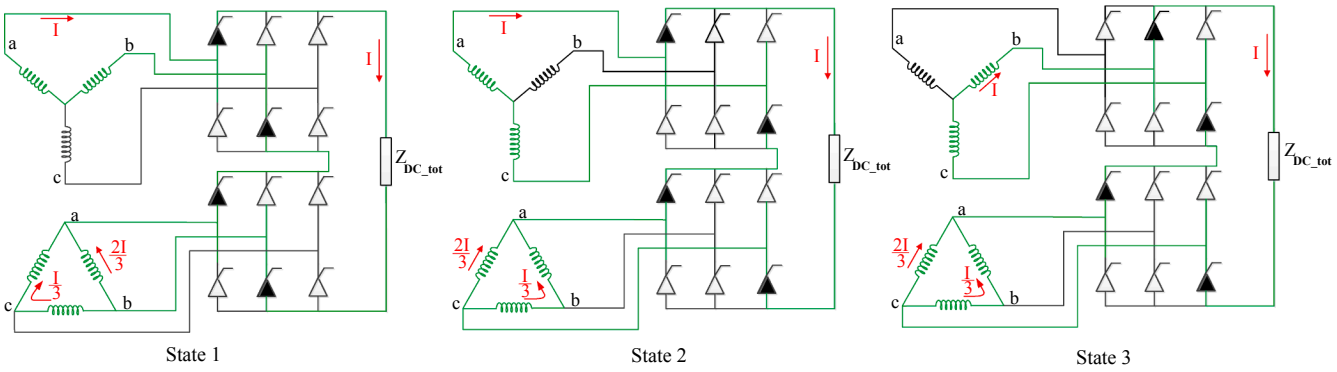

Fig. 5. Schematic illustration of three different states for phase "a" corresponding to modes 1,3,4 defined in Table 1.

normalized current waveform obtained from these equations, shown in Fig. 6(a), can be used as an alternative switching function given in Eq. (4) to find modulated AC current from DC current.

It should be noted that in this section winding losses have been neglected in these calculations for the sake of simplicity. By having step-wise transferred current values in AC side for one period (as shown in Fig. 6), the general form of the Fourier series for the current waveform on the AC side can be written as follows:

$$I_{md}(t) = I_1\cos(\omega t + \varphi_1) + \sum_{m=1}^{\infty} I_{12m\pm1}\cos([12m \pm 1]\omega t + \varphi_{12m\pm1}) \tag{11}$$

It can be shown that the modulated time-variant impedance transferred on the AC side should include 12n harmonics to represent the fundamental voltage waveform. Therefore, the general impedance form can be given as follows:

$$Z_m(t) = Z_0 + \sum_{n=1}^{\infty} Z_{12n}\cos(12n\omega t + \theta_{12n}) \tag{12}$$

where Z_m is the total modulated time-variant impedance of the converter seen from the AC side. Z_0 is the constant term of impedance, and the other terms are the modulating impedance terms with magnitudes of Z_{12n}. Assuming known grid voltage and current frequency components as illustrated before, the product of the impedance and the current function can be expanded and solved for each frequency to obtain the magnitude and phase of the corresponding impedance terms.

$$Z_0 \sum_{m=0}^{\infty} I_{12m\pm1}\cos([12m \pm 1]\omega t + \varphi_{12m\pm1}) + \sum_{n=1}^{\infty}\sum_{m=1}^{\infty} \frac{Z_{12n}I_{12m\pm1}}{2}\{\cos([12(n-m) \pm 1]\omega t + \theta_{12n} - \varphi_{12m\pm1}) + \cos([12(n+m) \pm 1]\omega t + \theta_{12n} + \varphi_{12m\pm1})\} = V_1\cos(\omega t + \varphi_{v1}) \tag{13}$$

The first term in this equation is the voltage drop across constant part of the modulated impedance, and the rest are voltage drop reflected from DC side imposed on AC side through higher frequency components of modulated impedance on the AC side. If terms with the same frequencies are separated, systems of nonlinear equations will be obtained within which magnitude and initial phase of impedance components are unknowns. In this study, impedance and current terms including frequency components of order less than 50 have been considered as the dominant terms. The trust region method (TRM) and Levenberg-Marquardt algorithms were evaluated and used to optimize unknown impedance components. These numerical iteration methods can be used to determine an accurate response within some repetition steps with objective function as low as 10^{-8}. Fig. 6 shows the modulated AC current and the time-variant impedance constructed from the optimization results, and their respective frequency spectrum.

The presence of characteristic harmonics of order $(12\ k \pm 1)^{th}$ on the AC side (as shown in Fig. 6(a)) has been demonstrated in Section 2. In this scenario, the conduction interval for each switch pair is equal, and the commutation overlap has not been considered. Therefore, as long as grid disturbances are not significant to disturb balanced switching conduction periods (small-signal analysis), the equivalent impedance obtained on the AC side will be accurate enough to assess the reflection of grid harmonics from the HVDC grid. Time-varying components of modulated impedance depend on the total DC side

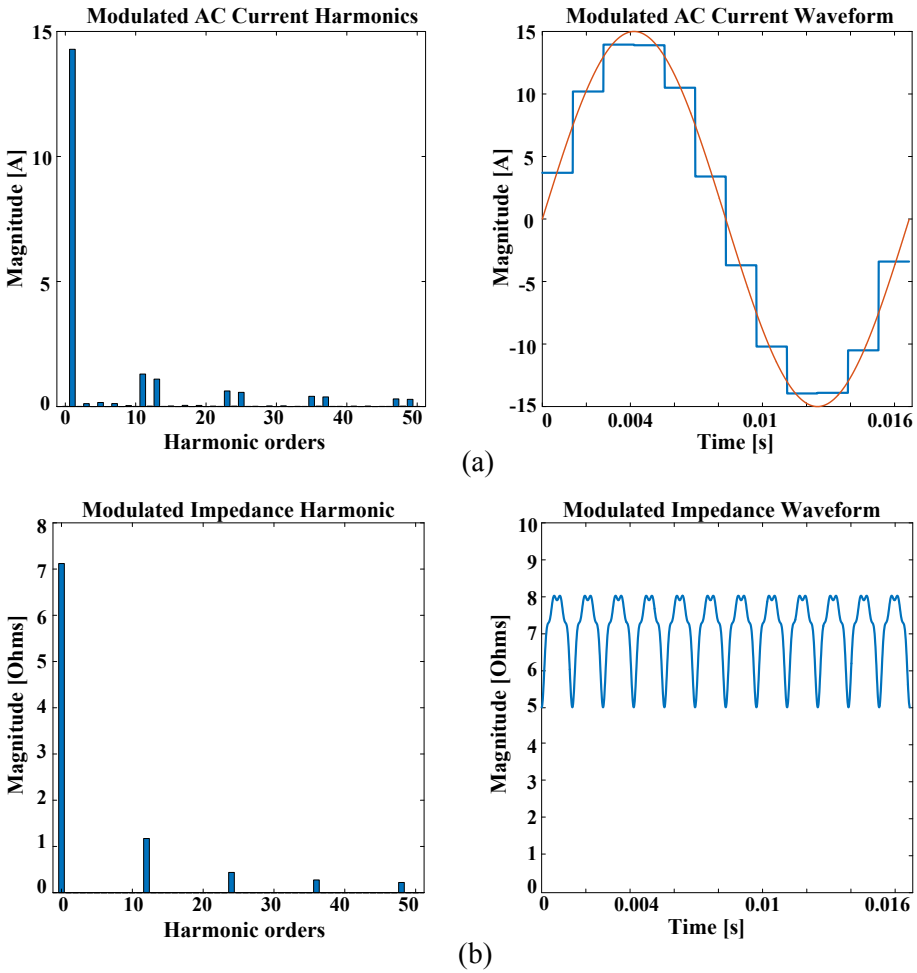

Fig. 6. Modulated current and calculated impedance seen on AC side with corresponding frequency spectrum (R,$L_{eq,DC}$ = 60 Ω, 288mH; R,$L_{leakage}$ = 0.5 Ω,6mH; turn ratio:0.5).

impedance and the switching function which is considered unaffected from disturbances; frequency-dependent time-independent terms depend on frequency and the sequences of the AC grid disturbances. The complete Norton equivalent model of the HVDC grid includes a current source representing all reflected harmonic components previously calculated in Eq. (11).

3.2.1.1. Modulated impedance calculation on AC side considering commutation overlap. In this section, the commutation overlap during phase transposition via converter switching has been considered and more accurate results are presented. Transformer leakage inductances have been considered in this case. Otherwise, high short circuit current would flow through windings during commutation overlap. Twelve overlapped switching modes (shown in Table 2) will occur in each fundamental cycle between conduction modes defined in Table 1.

Among these modes, four states are identified with different induced primary currents values in each phase as shown in Fig. 7, corresponding to modes 1,2,3, and 6 as defined in Table 2.

I_1, and I_2 are short circuit currents between transformer windings in Fig. 7. Similar calculations have been done in [15], so relevant equations have not been repeated here.

Having found the currents and induced voltages of the windings, then main current in circuit (1) can be obtained. Then, by using the general relation between voltages and currents of windings defined in Eq. (7), the primary AC current for each time interval can be obtained similar to the previous section. In [15], precise analysis was provided to represent the transfer of current between the two main conduction states during commutation overlap. Commutation overlap angle can be obtained with known induced voltages in secondary and tertiary windings, and transformer leakage inductances as defined in [15,25]. During this period, commutation current is gradually changing between conduction current steps obtained in the previous section. In this scenario, equation of similar general form as Eq. (11) can be defined for

Table 2
Overlapped switching modes in each period.

Connection modes	Occurred between modes in Table1	Secondary winding's phases			Tertiary winding's phases		
		a	b	c	a	b	c
1′	2 → 3	1		−1	1	−1	−1
2′	3 → 4	1	1	−1	1		−1
3′	4 → 5		1	−1	1	1	−1
4′	5 → 6	−1	1	−1		1	−1
5′	6 → 7	−1	1		−1	1	−1
6′	7 → 8	−1	1	1	−1	1	
7′	8 → 9	−1		1	−1	1	1
8′	9 → 10	−1	−1	1	−1		1
9′	10 → 11		−1	1	−1	−1	1
10′	11 → 12	1	−1	1		−1	1
11′	12 → 1	1	−1		1	−1	1
12′	1 → 2	1	−1	−1	1	−1	

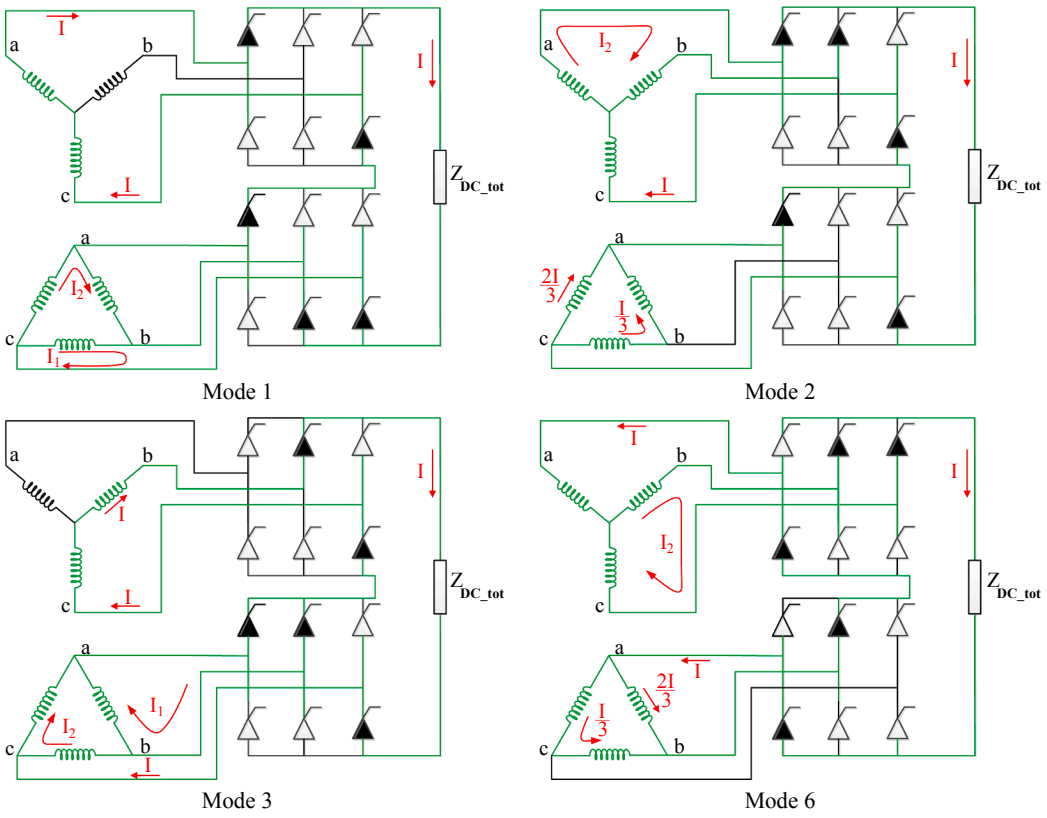

Fig. 7. -Schematic illustration of four different states for phase "a" corresponding to modes 1,2,3, and 6 defined in Table 2.

modulated current including $(12m \pm 1)^{th}$ harmonics. Taking the Fourier series of step-wise transferred current waveform, considering all 24 switching modes including all modes given in Table 1 and Table 2, provides magnitudes and initial phase of these harmonic components (as shown in Fig. 8(a)). By using the same procedure explained in section 3.2.1, components of the Fourier series of modulated impedances have been optimized through system of nonlinear equations for separated harmonics terms in each function via iterative optimization algorithms as outlined in Section 3.2.1.

By doing so, the transferred impedances on the primary side considering all 24 switching modes (defined in Tables 1 and 2) and its frequency spectrum are shown in Fig. 8. Smooth change of current in each step during commutation overlap angle is observed which reduces the magnitude of higher frequency components of the current and the modulated impedance with respect to the ideal switching condition described in the previous section. It means high-frequency components of equivalent impedance will reflect with lower magnitudes for disturbances induced in the AC grid at. Initial phase angle for each frequency component of the impedance is defined by a Fourier series of time-variant impedance. As stated earlier, the normalized current waveform in this section providing more accurate reflection function for AC current has been used to obtain modulated currents in the presence of harmonic disturbances.

3.3. Complete HVDC grid model for unbalanced harmonic disturbances

Since the reflection of injected harmonics on the AC side from the DC grid includes frequency components in different sequences, a positive and negative sequence model should be obtained and separated for further analysis. The product of the reflected current source in Norton equivalent (Eq. (4)) and the time-varying impedance illustrated in previous sections will present positive and negative sequences of voltage drops for different injected harmonics as have been modeled with sequence current dependent voltage sources in Fig. 9(b). Since harmonics either generated by saturated transformers during geomagnetic storm or reflected from the DC side follow the "natural" sequence relationship, harmonics of order $3k + 1$ and $3k + 2$ $(k = 0, 1, \cdots)$ are assigned to positive and negative sequences respectively which is not clear in their single-phase circuits and equations. That being so, the values of components in the circuits (shown in Fig. 9) can be mathematically delineated as shown below.

$$V_{PCC}(t) = V_1^{\pm}(t) + V_{nch}^{\pm}(t) \tag{14}$$

$$I_{md}(t) = I_1^{\pm}(t) + I_{ch}^{\pm}(t) + I_{nch}^{\pm}(t) \tag{15}$$

$$\begin{aligned} \upsilon(I_{md}) &= Z_{12k}(t)\cdot I_{md}(t) = Z_{12k}(t)\cdot[I_1^{+}(t) + I_{ch}^{\pm}(t)] \\ &\quad + Z_{12k}(t)\cdot[I_1^{-}(t) + I_{nch}^{\pm}(t)] \\ &= \upsilon_1^{\pm}(I_{md}) + \upsilon_{ch}^{\pm}(I_{md}) + \upsilon_{nch}^{\pm}(I_{md}) \\ &= \upsilon^{+}(I_{md}) + \upsilon^{-}(I_{md}) \end{aligned} \tag{16}$$

In these equations, $V_{PCC}(t)$, $V_1^{\pm}(t)$, $V_{nch}^{\pm}(t)$ are the voltage of point of common coupling, positive and negative sequences of (un)balanced fundamental voltage, and injected non-characteristic harmonics on AC side, respectively. Also, $I_{md}(t)$, $I_1^{\pm}(t)$, $I_{ch}^{\pm}(t)$, and $I_{nch}^{\pm}(t)$ are modulated current reflected to the AC grid, positive and negative sequences of the fundamental frequency current, and characteristic and non-characteristic components of the current, respectively. Current dependent voltage source $(\upsilon(I_{md}))$ is obtained from the time-varying term of the modulated impedance $(Z_{12k}(t))$ and the current $(I_{md}(t))$. Using all these parameters and Kirchhoff's equation, the impedance values for all existing frequency components $(Z_{md}^{\pm}(f))$ are calculated through an iterative algorithm. In the next section, accuracy of the impedance values obtained from this method has been compared with the direct method used in [14].

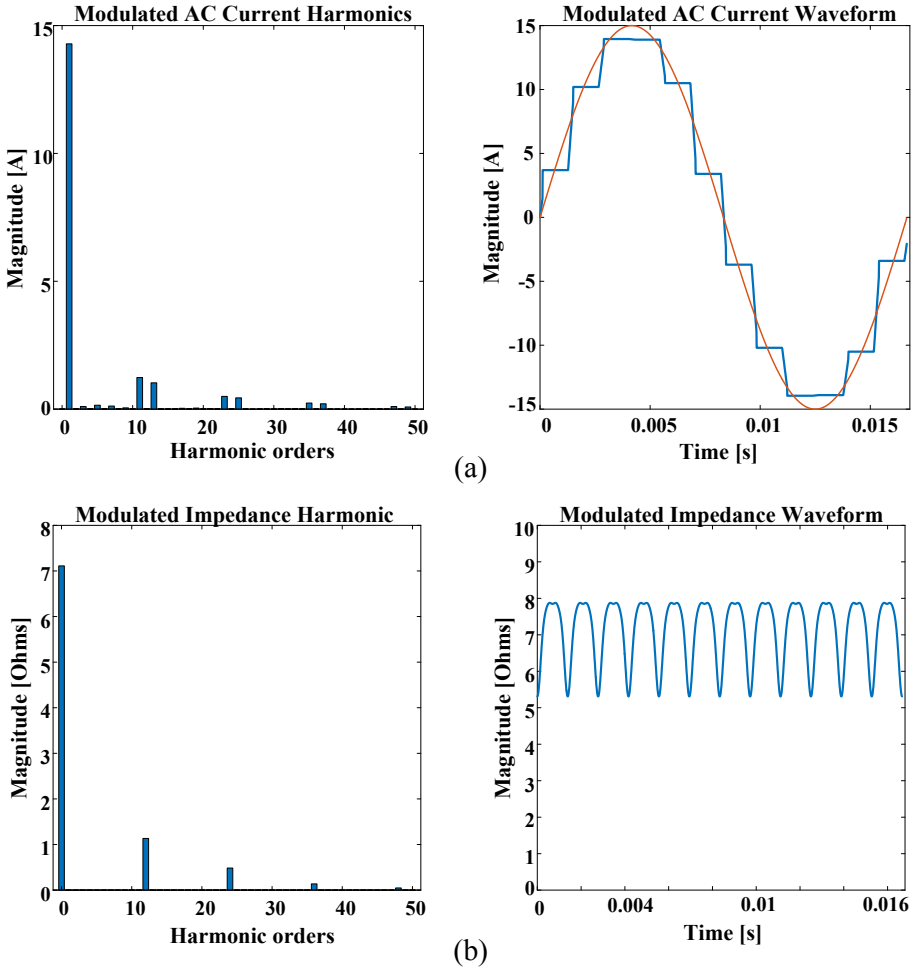

Fig. 8. Modulated current and calculated impedance seen on the AC side with corresponding frequency spectrum (R, $L_{eq,DC}$ = 60 Ω, 288mH; R,$L_{leakage}$ = 0.5 Ω,6mH; turn ratio:0.5, μ = 5°).

4. Application of proposed method and simulation results

Two simulation models have been investigated in this section to compare and verify the results. A complete HVDC grid model in EMTP including a DC transmission link using 12-pulse thyristor converters between two AC systems operating at 50 and 60 Hz with voltage ratings of 345 kV and 500 kV has been used to evaluate the impedance model proposed in this paper. This model has a complete control system to transmit 1000 MW (500 kV, 2kA) from a 60 Hz AC grid to a 50 Hz remote end AC grid (Fig. 10). AC filters have not been included so that all generated characteristic and non-characteristic harmonics in the AC and DC sides can be shown in voltage and current waveforms. Grid parameters used in the simulation are listed in Table 3.

In Fig. 11, the reflected voltage and current frequency components up to 30th order including characteristic and non-characteristic harmonics have been shown for the injected symmetrical second-order voltage harmonic ($V_2 = 0.1V_1$) in the primary AC system (60 Hz). Some noticeable harmonic components have been highlighted in the figure. All these harmonics have been categorized in Fig. 2. Harmonics of order 12n for 60 Hz and 120 Hz are observed on DC side, and harmonics of

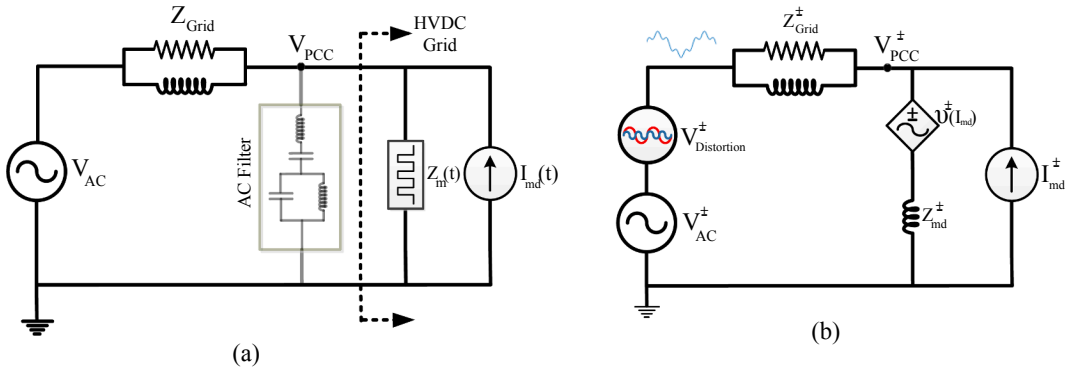

Fig. 9. (a) General equivalent model of Grid on AC side including HVDC grid model, (b) positive, negative sequence equivalent model of unbalanced and/or distorted grid.

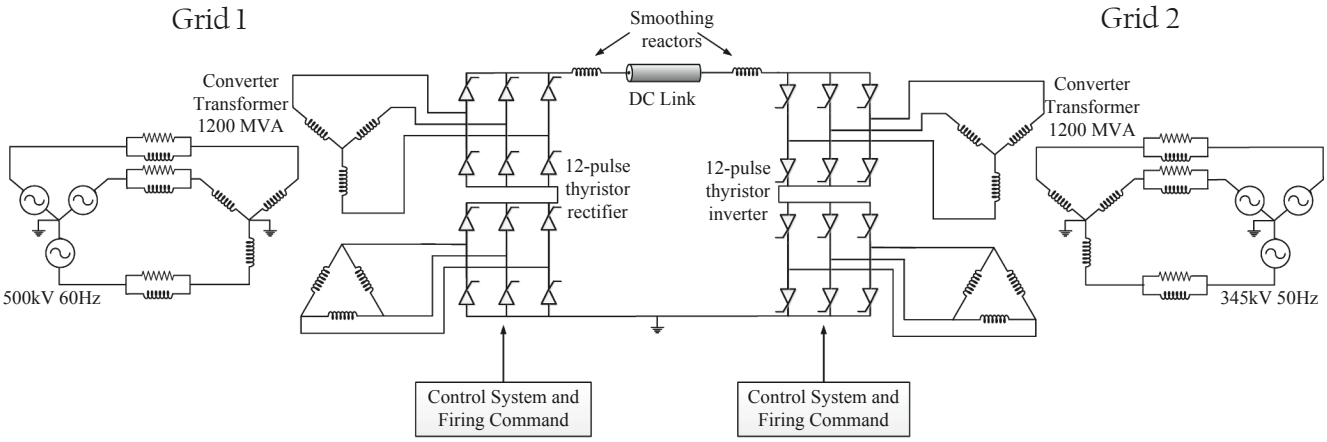

Fig. 10. Schematic diagram of simulated LLC-based AC/DC/AC system.

Table 3
Simulated model parameter in EMTP and MATLAB.

Grid parameters	values
Rectifier firing angles in steady-state	15°
Inverter firing angles in steady-state	139°
Converter transformer turn ratio (grid1)	450/200/200
Converter transformer turn ratio (grid2)	331/200/200
Line impedance (grid1)	13 Ω, 40mH
Line impedance (grid2)	6 Ω, 30mH
DC filter inductance in each side	200mH
DC link impedance	6.5 Ω, 40mH
Commutation overlap	5°

order 12n ± 1 and 12n ± 2 are generated on AC side.

The proposed analytical equivalent time-variant impedance model has been defined in MATLAB to calculate the reflected harmonic components on the AC and DC sides. To demonstrate the performance of this model, the frequency-dependent part of impedance in this model has been compared with the direct impedance method introduced in [14]. This direct method has been used for resonance phenomenon studies during geomagnetic storms on the specific Quebec-New England grid, and disregarded overlap angle and fast control of converter switches. System response to a small disturbance injected into the AC grid has been studied to find the reflection of DC impedance to the AC side. Additionally, Fourier analysis and modal transformation have been used in the EMTP simulated model to separate positive and negative sequences of voltage and current to obtain corresponding impedance and validate the two methods' results. Calculated impedance

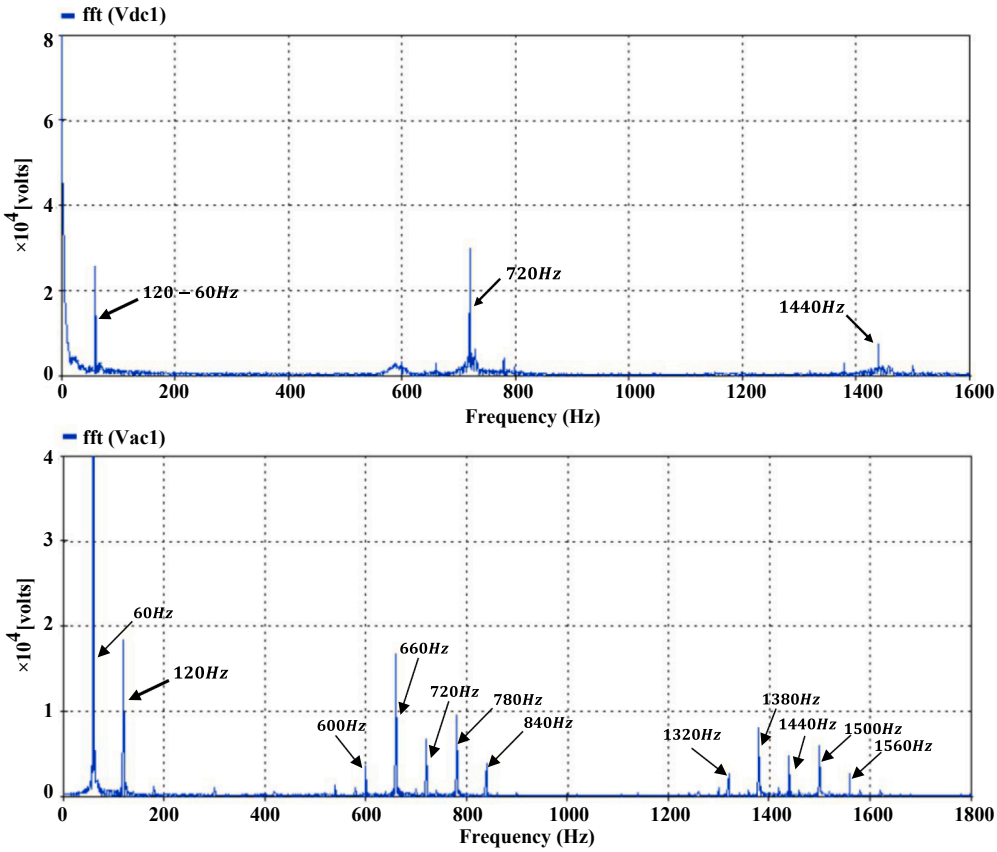

Fig. 11. Frequency spectrum of AC and DC voltages by injecting 10% second harmonic voltage through simulated system in EMTP.

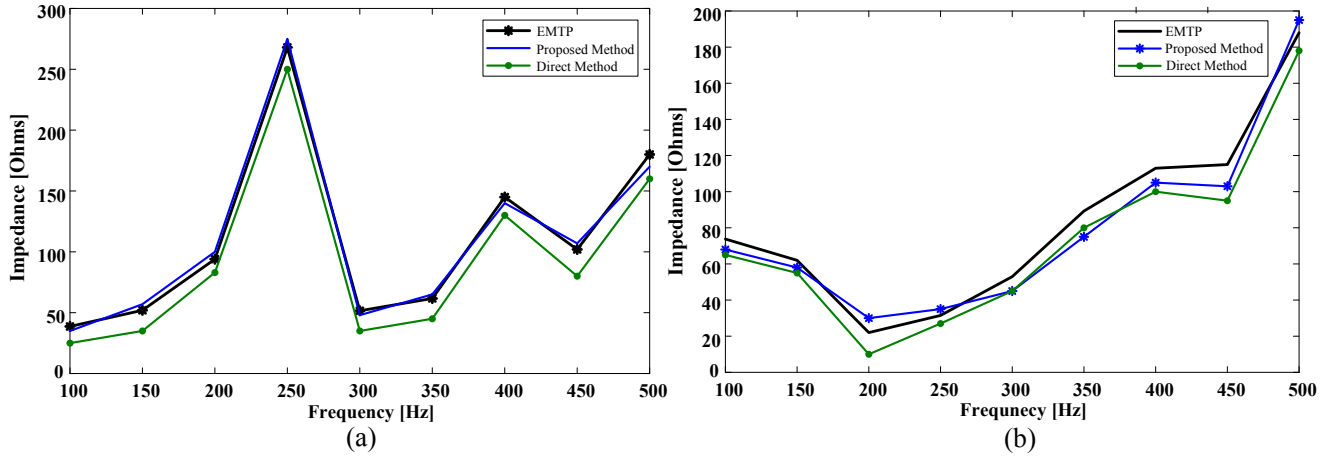

Fig. 12. AC side Equivalent impedance reflected from DC side: (a) positive sequence, (b) negative sequence.

for injected positive and negative sequences of voltage in the range of 100–500 Hz has been shown in Fig. 12.

Error produced by the proposed model is from the iterative optimization algorithm and is lower than error resulting from the direct method. Effectiveness of the proposed model has been demonstrated for the case of multiple injected harmonics due to transformer half-cycle saturation during a geomagnetic storm. Fig. 13 shows reflected impedance values for the worse case when the positive and negative sequences of voltage harmonics (4^{th+}, 7^{th+}, 9^{th+}, 2^{th-}, 5^{th-}, 7^{th-}) with the magnitude of 1 percent of fundamental voltage magnitude are applied simultaneously to the AC grid.

As can be seen, the obtained impedance of direct method is higher than the actual value. This is because the calculated impedance using this method is based on the reflection of a specific harmonic while disregarding the impact of other injected harmonics on the same frequency. As an example, an injected negative sequence second harmonic reflects the positive sequence fourth harmonic, and should be considered in the calculation of the reflected impedance of the fourth harmonic. Hence, reflected currents seen in direct method are lower and reflected impedance is higher. On the other hand, the proposed method is based on modulation theory as explained in Section 2, and all reflected harmonic components have been applied in objective functions to obtain optimized impedance values which provide more accurate results in the cases where multiple harmonic components have been superimposed on a power signal. The time-varying part of the impedance and the current source beside the reflected impedance (evaluated above) provide accurate modeling of HVDC grid and is used for grid disturbance analysis. To demonstrate the accuracy of the proposed complete equivalent model and compare its results of harmonic propagation with the complete EMTP grid model defined above, two scenarios have been considered and discussed here.

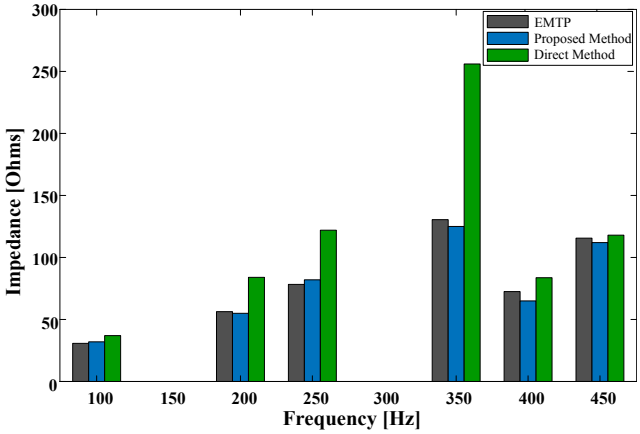

Fig. 13. Reflected equivalent impedance for multiple injected harmonics.

In the first scenario, an unsymmetrical second harmonic is applied to grid 1 near the power supply with phase voltages as follows:

$$V_a^1 = 500\angle 0 \quad V_b^1 = 500\angle -120 \quad V_c^1 = 500\angle +120$$

$$V_a^2 = 25\angle 0 \quad V_b^2 = 25\angle -150 \quad V_c^2 = 25\angle +150$$

Simulation results (DC modulated voltage and transferred AC current) provided by both models have been given in Table 4.

As can be seen, first and zero harmonic orders on the DC and AC sides, respectively, are non-characteristic harmonics due to the injected second harmonic on the AC sides. The rest of harmonics are characteristic harmonics.

In second scenario, a combination of harmonics (second to fifth harmonics) have been applied to simulate the half-cycle saturation of transformer during a geomagnetic storm resulting in odd and even harmonics in the grid. The unsymmetrical harmonic voltages applied to AC side are summarized in Table 5:

Dominant harmonics generated on the AC and DC sides have been shown in Table 6.

5. Conclusions

This paper presents a mathematical approach to obtain equivalent model based on modulated time-varying impedance concept for an HVDC grid and a remote end AC grid seen at the PCC of a local AC grid through a modulation process of a 12-pulse converter along with a three-winding converter transformer which is a commonly used configuration in point-to-point LCC-based HVDC topology for high power

Table 4
Results obtained from two models for injected second harmonic voltage.

Harmonic order (60 Hz fund.)	DC Voltage ($\frac{V_n}{V_1} * 100$)		Harmonic order (60 Hz fund.)	AC Current ($\frac{I_n}{I_1} * 100$)	
	Simulated Grid (EMTP)	Proposed model (Matlab)		Simulated Grid (EMTP)	Proposed model (Matlab)
0	100	100	0	1.8	1.6
1	2.65	2.5	1	100	100
3	1	0.7	2	1.9	1.7
12	2.3	2	11	6	5.6
24	2.7	2.4	13	4.4	4.1
			23	0.7	0.5
			25	0.5	0.3

Table 5
Applied three-phase voltage harmonics in the second scenario.

Harmonic Order	Phase A	Phase B	Phase C
First	$500\angle 0$	$500\angle -120$	$500\angle 120$
Second	$25\angle 0$	$25\angle 100$	$25\angle -100$
Third	$25\angle 50$	$25\angle -60$	$25\angle 70$
Forth	$25\angle -30$	$25\angle -120$	$25\angle 90$
Fifth	$25\angle -180$	$25\angle 60$	$25\angle -30$

Table 6
Results obtained from two models for injected voltage harmonics given in Table 5.

Harmonic order (60 Hz fund.)	DC Voltage ($\frac{V_n}{V_1} * 100$)		Harmonic order (60 Hz fund.)	AC Current ($\frac{I_n}{I_1} * 100$)	
	Simulated Grid (EMTP)	Proposed model (Matlab)		Simulated Grid (EMTP)	Proposed model (Matlab)
0	100	100	0	0.5	0.3
2	2.2	2	1	100	100
3	5.7	6	2	1.3	1.5
4	3.7	4.2	3	1.6	1.7
5	0.5	0.3	4	0.7	0.5
6	0.6	0.5	5	0.5	0.3
8	0.4	0.2	6	0.4	0.25
12	2.2	2.5	7	0.6	0.7
15	0.4	0.2	8	0.8	0.9
16	0.5	0.3	9	1.1	1.2
20	0.5	0.3	10	0.8	0.8
21	0.5	0.3	11	5.9	6
22	0.5	–	13	4.2	4
24	2.5	2.7	14	0.5	0.3
			15	0.5	0.3
			16	0.4	0.1
			23	0.7	0.5
			25	0.4	0.2

transmission between grids. Not only does it provide insight into the stability of the whole grid and a guideline for AC filter designers, but also the details regarding the grid reaction to a variety of harmonics generated due to half-cycle transformer saturation during geomagnetic storms. The ability to derive accurate equivalent model of a system allows high fidelity assessment of system vulnerability to different harmonic components, as well as the characteristics of these harmonics when damped (by providing higher series impedance or lower parallel impedance to ground) or excited (due to resonance near generated harmonics). The impact of commutation overlap on the modulation process has been considered. In addition, results obtained from the proposed equivalent model for optimized impedance values for the wide range of frequencies, reflected voltages, and reflected currents have been verified by the simulated grid model in EMTP.

Many authors have already addressed transferred harmonics for AC/DC configurations and presented quantitative generation of different groups of harmonics summarized in this paper. In some of these works, accurate calculation of current and voltage is required to find reflected current and voltage waveforms on both sides of converters using switching functions representing converter operation. Our proposed method provides the direct approach to calculate and evaluate the interaction of harmonics in the AC and DC grid. It should be noted that the total harmonic distortion is assumed to be not too high to have a significant impact on normal converter switching process; therefore, equidistant firing is assumed for switches. Also, since the main focus of this work is on the Line Commutated Converter (LCC) topology with high inductive DC filters, cross-modulation of harmonics transferred from the remote end converter has been neglected which will be addressed in future works for other converter configurations. Impedance-based stability analysis using proposed time-varying equivalent impedance models is another subject for our further investigation.

CRediT authorship contribution statement

Tohid Shahsavarian: Investigation, Software, Formal analysis, Visualization, Writing - original draft. **Yang Cao:** Conceptualization, Methodology, Supervision, Formal analysis, Project administration, Writing - review & editing. **Emmanouil Anagnostou:** Supervision, Project administration, Writing - review & editing. **Roderick Kalbfleisch:** Conceptualization, Resources, Validation, Funding acquisition, Writing - review & editing.

Declaration of Competing Interest

The authors declare that they have no known competing financial interests or personal relationships that could have appeared to influence the work reported in this paper.

Acknowledgement

The authors would like to thank the National Science Foundation (NSF) for funding support under Grant No. 1650544 and Eversource for partnership support through the Eversource Energy Center at the University of Connecticut.

Appendix A. Supplementary material

Supplementary data to this article can be found online at https://doi.org/10.1016/j.ijepes.2020.106173.

References

[1] Sun R, McVey M, Lamb M, Gardner RM. Mitigating geomagnetic disturbances. IEEE Electrification Mag 2015;3:34–45. 4.
[2] Mousavi SA, Bonmann D. Analysis of asymmetric magnetization current and reactive power demand of power transformers due to GIC. Procedia Eng 202-2017; 264-272.
[3] Juvekar GP, Davis K. MATGMD: A Tool for Enabling GMD Studies in MATLAB. IEEE Texas Power and Energy Conference (TPEC); 2019: 1–6.
[4] Sun R, Balch C. Comparison between 1-D and 3-D geoelectric field methods to calculate geomagnetically induced currents: a case study. IEEE Trans Power Deliv 2019;34(6):2163–72.
[5] Boteler DH, Pirjola RJ, Marti L. Analytic calculation of geoelectric fields due to geomagnetic disturbances: a test case. IEEE Access 2019;7:147029–37.
[6] Liu C, Wang X, Wang H, Zhao H. Quantitative influence of coast effect on geomagnetically induced currents in power grids: a case study. J. Space Weather Space Clim. 2018;8:A60.
[7] Haddadi A, Rezaei-Zare A, Gérin-Lajoie L, Hassani R, Mahseredjian J. A modified IEEE 118-bus test case for geomagnetic disturbance studies-Part I: model data. IEEE Trans Electromagn Compat 2019:1–11. https://doi.org/10.1109/TEMC.2019.2920271.
[8] Haddadi A, Rezaei-Zare A, Gérin-Lajoie L, Hassani R, Mahseredjian J. A Modified IEEE 118-bus test case for geomagnetic disturbance studies– Part II: simulation results. IEEE Trans Electromagn Compat 2019:1–10. https://doi.org/10.1109/TEMC.2019.2920259.
[9] Rezaei-Zare A, Etemadi AH. Optimal placement of GIC blocking devices considering equipment thermal limits and power system operation constraints. IEEE Trans Power Deliv 2018;33(1):200–8.
[10] Ngnegueu T, Marketos F, Devaux F, Xu T, Bardsley R, Barker S, et al. Behavior of transformers under DC/GIC excitation: phenomenon, impact on design/design evaluation process and modeling aspects in support of design. Cigre 2012.
[11] Taylor J. Assessment guide: GMD harmonic impacts and asset withstand capabilities. EPRI Final Report (3002006444); 2016.
[12] Bozoki B, Chano SR, Dvorak LL, Feero WE, Fenner G, Guro EA, et al. The effects of GIC on protective relaying. IEEE Trans Power Delivery 1996;11:725–39.
[13] Sood VK. HVDC and FACTS Controllers- Applications of Static Converters in Power Systems. Kluwer Academic publishers; 2004.
[14] Dickmander DL, Lee SY, Desilets GL, Granger M. AC/DC harmonic interactions in the presence of GIC for the Quebec-New England Phase II HVDC transmission. IEEE Trans Power Delivery 1994;9:68–78.
[15] Wood AR. An analysis of non-ideal HVDC convertor behaviour in the frequency domain, and a new control proposal. PhD Thesis 1993, University of Canterbury.
[16] Hu L, Yacamini R. Harmonic transfer through converters and HVDC links. IEEE Trans Power Electron 1992;7:514–25.
[17] Larsen EV, Baker DH, McIver JC. Low-order harmonic interactions on AC/DC

systems. IEEE Trans Power Deliv 1989;4:493–501.
[18] Horton R. High-Altitude Electromagnetic Pulse and the Bulk Power System: Potential impacts and mitigation strategies. EPRI 2019:3002014979.
[19] Nazir M, Burkes K, Enslin JHR. Converter-based Power System Protection against DC currents in Transmission and Distribution Networks. IEEE Trans Power Electron 2020;35(7):6701–4. https://doi.org/10.1109/TPEL.2019.2963313.
[20] Hu L, Ran L. Direct method for calculation of AC side harmonics and interharmonics in an HVDC system. IEE Proc - Gener, Trans Distrib 2000;147:329–35.
[21] Liu C, Bose A, Tian P. Modeling and analysis of HVDC converter by three-phase dynamic phasor. IEEE Trans Power Deliv 2014;29:3–12.
[22] Hu L, Yacamini R. Calculation of harmonics and interharmonics in HVDC schemes with low DC side impedance. IEE Proc C - Gener, Trans Distrib 1993;140:469–76.
[23] Hu L, Morrison RE. The use of modulation theory to calculate the harmonic distortion in HVDC systems operating on an unbalanced supply. IEEE Trans Power Syst 1997;12:973–80.
[24] Hume DJ, Wood AR, Osauskas CM. The effect of AC system impedance on the cross-modulation of distortion in HVDC links. In: 10th International Conference on Harmonics and Quality of Power. Proceedings 2002; 1: 196-201.
[25] Jovcic D, Ahmed K. High voltage direct current transmission-converters, systems and DC grids. John Wiley & Sons Inc; 2016.